AIP | Journal of Applied Physics

Beneficial roles of Al back reflectors in optical absorption of Si nanowire array solar cells

Eunsongyi Lee, Keya Zhou, Minji Gwon, Jin-Young Jung, Jung-Ho Lee, and Dong-Wook Kim

Citation: Journal of Applied Physics **114**, 093516 (2013); doi: 10.1063/1.4820525
View online: http://dx.doi.org/10.1063/1.4820525
View Table of Contents: http://scitation.aip.org/content/aip/journal/jap/114/9?ver=pdfcov
Published by the AIP Publishing

Beneficial roles of Al back reflectors in optical absorption of Si nanowire array solar cells

Eunsongyi Lee,[1] Keya Zhou,[2] Minji Gwon,[1] Jin-Young Jung,[2] Jung-Ho Lee,[2,a)] and Dong-Wook Kim[1,b)]
[1]*Department of Physics, Ewha Womans University, Seoul 120-750, South Korea*
[2]*Department of Chemical Engineering, Hanyang University, Ansan 426-791, South Korea*

(Received 21 July 2013; accepted 21 August 2013; published online 6 September 2013)

We investigate the influence of Al back reflectors on the optical absorption spectra of Si nanowire (NW) arrays by using the finite-difference time-domain simulation method. A flat Al layer enhances the absorption in the NW array due to not only the reflection-induced optical path length enlargement but also reflection of light between NWs and localized surface plasmon induced optical field confinement. An Al underlayer with a grating structure allows grating-coupled surface plasmon polariton excitation and raise the optical absorption in the Si NWs. Interplay among all these factors on the optical absorption and expected solar cell performance of the NW arrays is discussed. © *2013 AIP Publishing LLC*. [http://dx.doi.org/10.1063/1.4820525]

I. INTRODUCTION

Semiconductor nanowires (NWs) have broad-band and outstanding light-trapping properties. The intriguing optical characteristics of the NWs have been attributed to various phenomena, including the resonant guided mode,[1,2] whispering gallery mode,[3] and Fabry-Perot interference.[4] The resonant modes and resulting absorption spectra depend on the physical parameters of an individual NW, such as diameter, length, and dielectric constant. In NW arrays (an assembly of NWs), the period, filling ratio, and structural randomness (geometry of NW and spacing between NWs) can further influence their optical properties.[5–17] Such unique optical characteristics of semiconductor NWs have encouraged us to investigate NW-based optoelectronic devices.[1–23]

The omni-directional and enhanced optical absorption of the NW arrays ensures high efficiencies of NW-based solar cells all day long.[5–14] In addition to such optical advantages, wire-based solar cells with radial *p-n* junctions can have close-to-unity carrier collection probability, when the diameter of the wire is smaller or comparable to the minority carrier diffusion length.[5] As already demonstrated, fabrication of flexible devices is also possible using low-cost and large-area wire formation processes.[5,14] In spite of such expectations, the efficiencies of the wire-based solar cells still have not surpassed those of the planar devices. Serious surface and interface recombination has been regarded as a major obstacle in raising the energy conversion efficiency.[15] Practically, it is a formidable task to suppress recombination and resulting carrier collection loss in the wire arrays with large surface-to-volume ratio.

One of the simplest ways to reduce the recombination loss is to use shorter NWs with less surface area. All the fabrication processes for absorber structures with less surface area, including conformal doping and passivation, and top-contact formation, will be easy.[24] However, the small optical thickness will seriously limit the ultimate energy conversion efficiency. Thin film solar cell technologies have established several light trapping strategies, such as anti-reflection coating, surface texturing, and back-surface optical reflection.[25] The first and second ones lower optical reflection at the front surface. The last one increases the optical path length in the absorber. The NW array possesses extremely low reflectance, and hence reflection loss is not a big concern. Implementation of the back reflector is helpful to increase the optical path length and raise the efficiency of short NW solar cells. The conducting back reflector also works as back contact to collect the carriers and flow them to an external load, as already demonstrated in solar cell and photodetector applications.[5,14,20]

Surface plasmon (SP), collective oscillation of conduction electrons at the metal/dielectric interface, should be considered to explain the optical properties of the nano-scale metal/semiconductor contacts.[16–23] SP excitation can confine the light and increase the optical absorption, which can drastically alter the absorption spectra of the NW array with the metallic back reflector. SPs also can cause intrinsic absorption loss in the metal nanostructure itself.[16,26] Therefore, studies on the optical characteristics of NW array with the metal back reflector will be interesting and important to improve the device architecture of the wire-based solar cell.

In this work, we investigated the optical characteristics of Si NW arrays with and without Al underlayers by simulations. A flat Al underlayer beneath the Si NW array enhanced the optical absorption in wide wavelength range. The Al layer reflected the light between NWs as well as the light in NWs, which increased the optical path length in the NWs. In addition, localized SP (LSP) at the NW/Al interface enhanced absorption in the NWs. When the Al underlayers had periodic structures, grating-coupled surface plasmon polaritons (SPPs) enabled the NW array to have additional absorption peaks for sparse and small-diameter arrays. The expected maximum photocurrent of the NW array with the

a)Author to whom correspondence should be addressed. Electronic mail: jungho@hanyang.ac.kr
b)dwkim@ewha.ac.kr

back reflector was larger than that of the equal-thickness planar counterpart.

II. SIMULATION

To describe the electromagnetic field distribution in NW arrays, the Maxwell equations were solved by the finite-difference time-domain (FDTD) method. In this study, the NW arrays were modeled in FDTD (Lumerical FDTD Solutions) as a unit cell embedded in air with perfectly matched layers (PMLs) on the top and bottom, and with periodic boundary conditions at the sidewalls (Fig. 1).[27,28] The diameter of the Si NW was varied from 60 to 400 nm, and the length was fixed to be 1 μm. Several kinds of NW arrays were considered in our simulation, as illustrated in Fig. 1. The first type had only Si NWs without any underlayer (hereafter called as type [A]). The second and third types had 60-nm-thick conducting underlayers with a flat surface and a grating structure, respectively. For the last type, the grating period was the same of the NW array period (P) and the width of the upper part grating (W) was set to be the half of P. The height of the grating was 30 nm and the height of the flat layer under the grating was also 30 nm. As shown in Fig. 1, the polarization and propagation directions of the incident light were parallel to the x-axis and z-axis, respectively. The absorption in Si NWs was estimated by measuring the amount of power flowing into and out of NWs. When the NW arrays were on the Al conducting layers, the absorption in the Al layer as well as the absorption in the NW array was estimated by putting two monitors above and below the Al layer.

III. COMPASIRON OF A THIN FILM AND A NW ARRAY

Figure 2(a) shows optical absorption (A) spectra of type [A] (diameter: 100 nm, length: 1 μm, and period: 800 nm) and a 1-μm-thick Si thin film. The absorption of type [A] and the thin film decreases with increasing wavelength because of a low absorption coefficient of Si for long-wavelength light. The reflected light waves at the top and bottom of the Si/air interfaces interfere with each other, resulting in the Fabry-Perot interference and oscillatory behaviors of the absorption spectra.[13] The oscillation amplitude diminishes at short wavelengths, since the interference effect becomes less dominant due to short penetration depth.

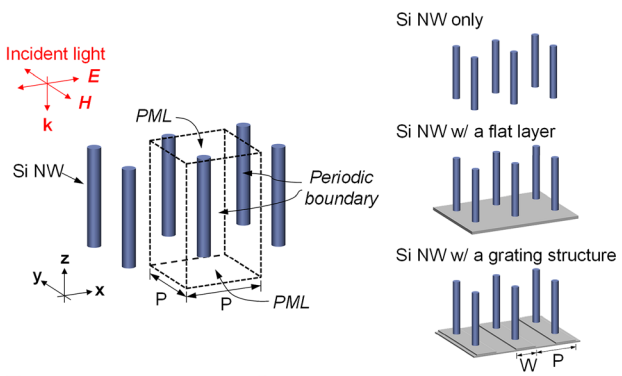

FIG. 1. Schematic illustration of the NW array used in the FDTD simulation and different types of the NW arrays with and without underlayers.

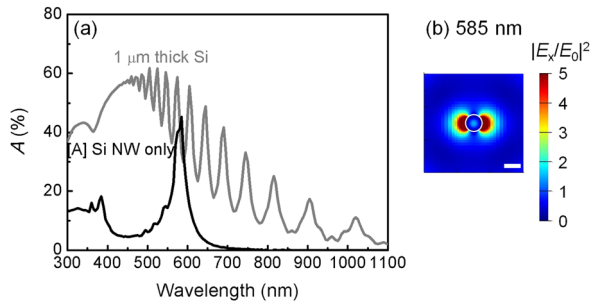

FIG. 2. (a) Simulated optical absorption (A) spectra of a 1-μm-thick Si thin film and a Si NW array (diameter: 100 nm, length: 1 μm, and period: 800 nm) and (b) cross-sectional distribution of $|E_x/E_0|^2$ at $\lambda = 585$ nm of a single NW ($|E_0|^2$: the intensity of incident light). Scale bar is 100 nm.

The absorption of the 1-μm-thick Si has maximum at intermediate wavelength (λ) range, ~450 nm.

Type [A] shows much less absorption in the whole simulation wavelength range than the thin film. The volume fraction of the NWs is only 1% of that of the continuous equal-thickness film. In spite of such a small volume, the absorption peak at $\lambda = 585$ nm is as large as 45%. Figure 2(b) shows the electric field distribution in the Si NW at $\lambda = 585$ nm, indicating an effective coupling of incoming light to the fundamental guided mode ($HE_{1,1}$ mode) supported by NW.[1] The resonant guided mode can dramatically increase the absorption cross-section of NW. The small amplitude oscillatory feature in the NW absorption is due to the interference in NWs, as is the case of the thin film.

IV. INFLUENCE OF A FLAT ALUMINUM UNDERLAYER

Figures 3(a) and 3(e) compare absorption spectra of types [A] and a Si NW array (diameter: 100 nm, length: 1 μm, and period: 800 nm) with a 60-nm-thick flat Al underlayer (hereafter called as type [B]): the overall absorption of type [B] is larger than that of type [A]. Both samples have maximum absorption at $\lambda \sim 600$ nm. Type [A] has a single peak at $\lambda \sim 585$ nm, originated from the guided mode resonance [Fig. 2(b)]. The difference in the absorption of types [A] and [B] (hereafter, denoted as [B]-[A]) shows a maximum value at $\lambda \sim 600$ nm and positive values in wide spectral range.

For better understanding, a Si NW/Al-disk array (type [C]) is also studied. The diameter and the thickness of the Al disk are identical to that of the NW and that of the flat Al underlayer, respectively. As shown in Fig. 3(b), the absorption of type [C] has closely spaced two peaks. The larger and sharper peak at 595 nm can be attributed to the resonant guided mode, just like the peak of type [A]. Another peak at 635 nm is much broader than the peak at 595 nm, whose physical origin will be discussed later. It can be also noted that the absorption of type [C] at $\lambda < 600$ nm is almost identical to that of type [A], as clearly seen from [C]-[A] [Fig. 3(f)]. Both the Al disk in type [C] and the continuous Al layer in type [B] will reflect light in NWs. However, it should be noted that the absorption of type [C] is very different from that of type [B]. This indicates that the absorption

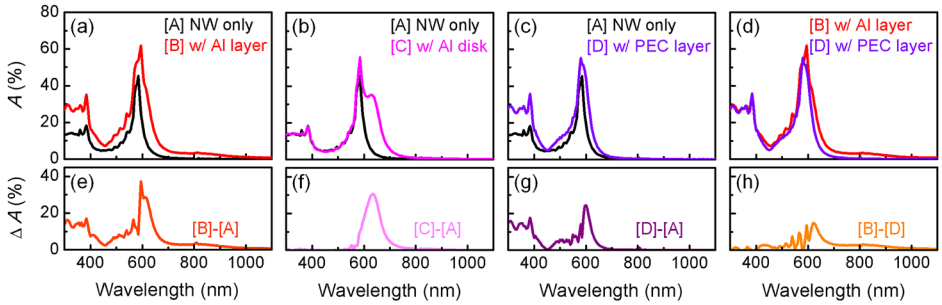

FIG. 3. (a)–(c) Simulated optical absorption (A) spectra of 100-nm-diameter Si NW arrays without any underlayer (type [A]), with a flat Al underlayer (type [B]), and with a perfect electric conductor (PEC) layer (type [D]). (d) A of a Si NW/Al-disk array (type [C]) is also compared. (e)–(h) The difference in the optical absorption of four different pairs.

spectrum of type [B] cannot be solely explained by the increase of the optical path length.

Type [D] corresponds to a Si NW array with a perfect electrical conductor (PEC) underlayer. Type [D] has maximum absorption at $\lambda \sim 600$ nm, and the absorption of type [D] is larger than that of type [A] in the whole simulation wavelength range. As shown in Fig. 3(g), [D]-[A] has the largest value at $\lambda \sim 600$ nm and has the second largest value at $\lambda < 400$ nm.

It can be noted that both of types [B] and [D] have larger absorption at $\lambda < 400$ nm than types [A] and [C]. Only small portion of short wavelength light could reach the conducting underlayer (e.g., penetration depth of Si, $\delta = 1.08\,\mu$m at $\lambda = 550$ nm), and hence reflection of the light propagating through the NWs cannot significantly contribute to the increase of the absorption in the short wavelength region. The field pattern around the NWs is quite different from that of the incident light, as shown in Fig. 4(a). The Si NWs significantly distort the wavefront and the Poynting vector of the incident light is not perpendicular to the surface of the Al layer. As a result, the light between NWs can be absorbed in the sidewalls of NWs. This can explain relatively large optical absorption in type [A] at $\lambda < 400$ nm (>10%) in spite of its very small filling ratio (~1%). In addition, the continuous conducting underlayers in types [B] and [D] can reflect the light between NWs, further raising the absorption. The Al disk cannot efficiently reflect such light between NWs and hence the absorption of type [C] at $\lambda < 400$ nm is similar to that of type [A].

Figure 3(d) compares optical absorption spectra of types [B] and [D]. Reflectance of light by the PEC layer will not be less than that by the Al layer. However, [B]-[D] has positive values in wide wavelength range (mainly at $\lambda > 400$ nm), as shown in Fig. 3(h). These results suggest that the optical reflection alone cannot completely explain the spectral behavior of type [B].

Figure 4(a) shows that very large electric field intensity is observed in the NW bulk of type [B] at $\lambda = 595$ nm. This suggests that the 595-nm-peak should be originated from the guided mode resonance, as expected. The existence of the Al underlayer does not significantly vary the resonant guided-mode peak position, which is mainly dependent on the NW diameter.[1,2] The electric field patterns of type [B] at $\lambda = 610$ nm and type [C] at $\lambda = 635$ nm are similar: both have strongly confined field at the Si NW/Al interface and the maximum field intensity is more than 100 times larger than that of the incident light. Such localized field confinement at the semiconductor/metal interface suggests the LSP excitation.[15–22,27–30] The strongly concentrated optical field at the NW/Al interface can cause the absorption peaks of type [B] at $\lambda = 610$ nm and type [C] at $\lambda = 635$ nm, as clearly seen from [B]-[A] and [C]-[A] in Figs. 3(e) and 3(f). The PEC layer cannot allow the LSP excitation, and hence the absorption peak of type [D] is almost the same of that of type [A] (see Figs. 3(g) and 3(h)). Thus, it should be noted that the absorption spectrum of type [B] has closely spaced two peaks with distinct physical origins.

Figure 4(b) shows schematic illustrations for the three major factors of the absorption enhancement in the NW array with the Al back reflector: (1) reflection of light in NWs, (2) reflection of light between NWs, and (3) optical field confinement due to the plasmonic effect. For quantitative comparison, maximum achievable short-circuit current density (J_{sc}) of the NW arrays were estimated from the following equation:

$$J_{sc} = \int_{300\,\mathrm{nm}}^{\lambda_g} I(\lambda)A(\lambda)\frac{e\lambda}{hc}d\lambda, \qquad (1)$$

where λ is wavelength, $I(\lambda)$ is the AM 1.5 solar spectral irradiance, $A(\lambda)$ is the Si absorption, and λ_g is the wavelength corresponding to the band gap of Si (1100 nm).[6] J_{sc} values of type [B] (4.36 mA/cm^2) is 40% larger than that of type [D] (3.11 mA/cm^2). Such significant increase of J_{sc} manifests the plasmonic effects of the back reflector in the NW solar cells.

Figure 5 shows the positions of the LSP resonance (LSPR)-induced peaks in the absorption spectra of type [B]

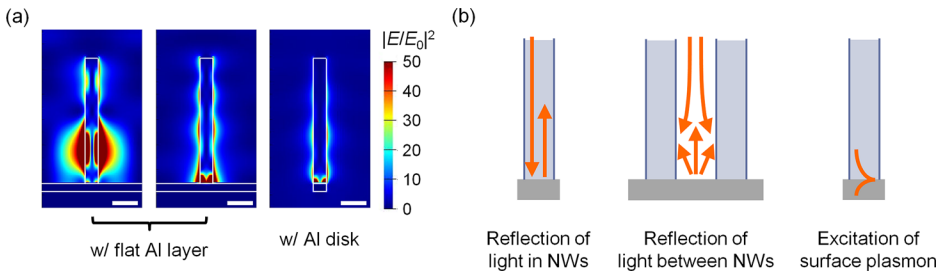

FIG. 4. (a) Cross-sectional electric field intensity distributions at $\lambda = 595$ and 610 nm for a single Si NW in type [B], and at $\lambda = 635$ nm for a single Si NW in type [C] ($|E_0|^2$: the intensity of incident light). Scale bars are 200 nm. (b) Illustration of three major factors of the Al back reflector to raise the optical absorption in the NW array.

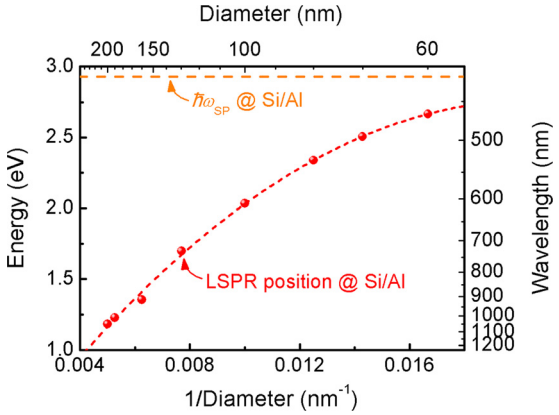

FIG. 5. Positions of the LSPR-induced absorption peaks as a function of the NW diameter. Red dots and a red dotted line correspond to the data taken from the absorption spectra and a visual guide line, respectively. ω_{SP} indicates the SP resonance frequency at the Si/Al interface.

as a function of the Si NW diameter. The peak moves to longer wavelengths with increasing NW diameter and the frequency of the peak is inversely proportional to the NW diameter for large diameters. The depolarization field in the larger Al disk becomes smaller, so that the LSPR frequency becomes smaller.[27–29] At a small diameter limit, however, material characteristics are predominant and the LSP excitation frequency approaches the SP resonance frequency at the Si/Al interface (ω_{SP}). Such diameter dependence assures the LSPR effects in the optical absorption spectra of the NW arrays with the Al back reflector.

V. INFLUENCE OF AN ALUMINUM GRATING STRUCTURE

Figure 6(a) shows the absorption spectra of types [A] and a NW array with an Al grating structure with period of 800 nm (type [E] see the schematic diagram in Fig. 1). Overall absorption of type [E] is larger than that of type [A]. Type [E] has larger absorption than type [A] at <700 nm, which can be attributed to the reflection and LSPR, similar to the case of type [B]. Shape and magnitude of [E]-[A] at 500 nm $< \lambda <$ 700 nm is similar to [B]-[A], implying comparable LSPR contribution. In addition, type [E] has a new peak at $\lambda = 815$ nm as shown in Figs. 6(a) and 6(b). In such near infrared (NIR) region, the absorption of type [A] is negligibly small but the absorption of type [E] is as large as 8.9%. Such increase is remarkable, since the penetration depth in the NIR region is much longer than the Si NW length.

Figures 6(c) and 6(d) show the cross sectional electric field distributions of types [A] and [E] at $\lambda = 815$ nm, respectively. The grating structure drastically modifies the field pattern and the intensity around the NWs. The field distribution of the grating only (without Si NWs) reveals a strong field formation at the grating edges, as shown in Fig. 6(e). The Al grating can excite SPPs at the air/Al interface.[20,31] The grating-coupled SPP propagates along the air/Al interface and partially scatters into the free-space mode at the edge of the grating. Such scattered light as well as the propagating SPPs can transfer energy to the Si NWs and enhance their optical absorption. Here, we should note that all the calculation results in Figs. 6(a)–6(e) were obtained for the TM mode (i.e., x-polarization) incident light. The absorption spectra of type [E] under the TE mode (i.e., y-polarization) illumination did not have a NIR peak. This assures us that the NIR peak is originated from the SPP excitation.

The relation between the wavevector and frequency of the grating-coupled SPPs can be obtained according to Eq. (2)

$$k_x = \frac{\omega}{c}\sin\theta \pm n\frac{2\pi}{P}, \tag{2}$$

where P is the grating period and n is an integer.[31] The SPP-related absorption peaks (dark blue triangles in Fig. 7) are consistent with the calculation results from Eq. (2) (a cyan line in Fig. 7). The grating period determines the SPP-induced absorption peak positions. This shows that we can tune the optical spectral response of type [E] as desired by varying the grating period.

VI. 400-NM-DIAMETER NW ARRAY

Figure 8(a) shows optical absorption spectra of 400-nm-diameter NW arrays (length: 1 μm and period: 800 nm) with and without an Al underlayer. According to recent numerical studies, such array is close to optimal one to achieve the high efficiency of the wire-based solar cell.[6,7] The absorption spectra of the large-sized NW array are more complicated than those of the small-sized NW array, as carefully discussed in a recent article of Sturmberg *et al.*[13] Obviously, the Al underlayer increases the overall absorption of the NW array. The absorption at short wavelengths of the NWs with the flat Al layer is larger than that of the NWs only. Such

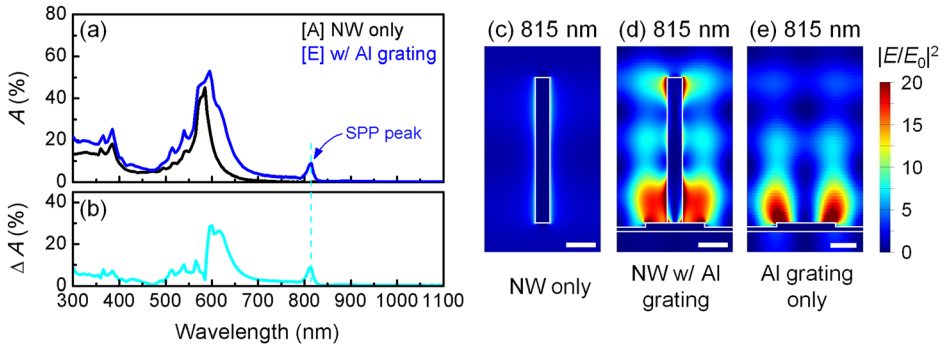

FIG. 6. (a) Simulated optical absorption (A) spectra of 100-nm-diameter Si NW arrays without an Al underlayer (type [A]) and with an Al grating structure (type [E]). (b) Difference in the optical absorption of type [A] and type [E]. Cross-sectional electric field intensity distributions at $\lambda = 815$ nm for a single Si NW in (c) type [A] and (d) [E], and (e) Al grating only without NW ($|E_0|^2$: the intensity of incident light). Scale bars are 200 nm.

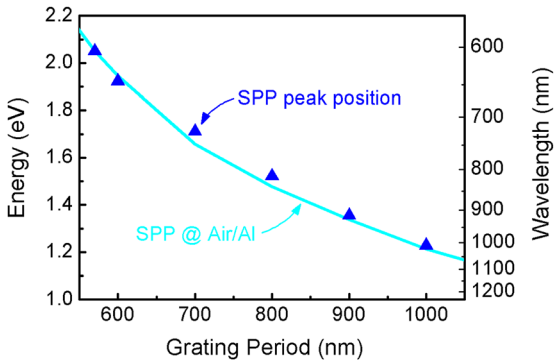

FIG. 7. Positions of SPP-related absorption peaks (symbols) taken from the simulated spectra, as a function of the grating period. A line corresponds to grating-coupled SPP energy, expected from the dispersion relation of SPP at air/Al interface and the grating period [Eq. (2)].

difference can be explained by the reflection of light between NWs by the back reflector.

The Al underlayer also increases the long-wavelength absorption of the NW array, except for narrow wavelength region (e.g., $\lambda \sim 850$ nm). Figure 8(a) also shows the absorption of the Al underlayer as well as the absorption of the NWs. Figures 8(b)–8(d) show the cross sectional electric field distributions at some of the peak wavelengths in the Al absorption. The field patterns exhibit strong field enhancement at the NW/Al interface, clearly indicating the LSP excitation. The number of nodes increases as decreasing the wavelength, revealing higher order LSP mode formation. Even at such wavelengths where the LSPR at the Si/Al interface occurs, the absorption of the NWs with the Al layer is comparable to or larger than that of the NWs without the Al layer. This means that the LSP excitation can enhance the overall absorption in the NWs in spite of the parasitic absorption loss in the Al layer. Figure 8(a) reveals that the notable plasmonic absorption in the Al layer occurs at the wavelength region somewhat far from the peak in the solar spectrum. This shows that the Al back reflector would not cause significant drop of the photocurrent in the Si NW solar cell.

Figure 9 shows calculated J_{sc} values for several types of 400-nm-diameter NW arrays with various periods (400–800 nm) obtained from Eq. (1). As expected from Fig. 8,

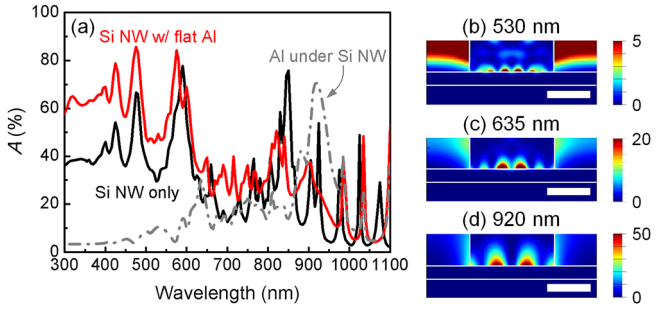

FIG. 8. (a) Simulated optical absorption (A) spectra of 400-nm-diameter Si NW arrays with and without a 60-nm-thick flat Al underlayer, and A of the Al layer under the Si NWs. Cross-sectional distribution of the electric field intensity, $|E/E_0|^2$, at $\lambda =$ (b) 530 nm, (c) 635 nm, and (d) 920 nm at the Si NW/Al interface ($|E_0|^2$: the intensity of incident light). Scale bars are 200 nm.

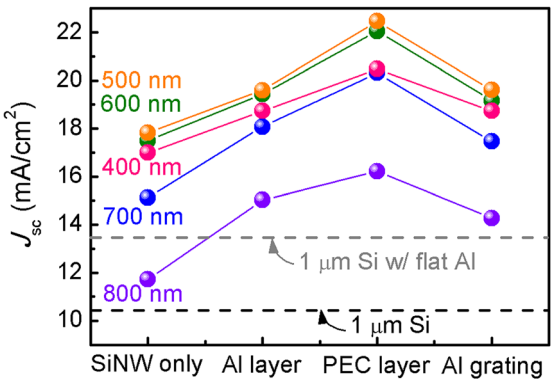

FIG. 9. Calculated short-circuit current densities, J_{sc}, for several types of 400-nm-diameter NW arrays with various periods (400-800 nm). Gray and black dashed lines indicate J_{sc} of the 1-μm-thick Si with and without the flat Al underlayer, respectively.

J_{sc} of the NW array with the flat Al layer (15.0 mA/cm^2) is much larger than that of the NW array without the Al layer (11.7 mA/cm^2). Comparison of PEC and Al can clarify the SP effect, since the PEC boundary condition doesn't allow the SP excitation. J_{sc} of the 400-nm-diameter NW array with the PEC back reflector (16.2 mA/cm^2) is about 8% larger than that with the Al back reflector. This reveals that the absorption in the Al back reflector doesn't seriously deteriorate the total photocurrent of the Si NW solar cell, as discussed above. Decrease of the period (P) can raise J_{sc} of the NW array with the Al back reflector, and J_{sc} for $P = 500$ nm is as large as 19.6 mA/cm^2 (45.2% larger than that of 1-μm-thick Si with a flat Al back reflector). Further decrease of the period (for example, $P = 400$ nm) lowers J_{sc}, since a NW array with a larger filling ratio will lose the geometrical optical gain and behaves more like a continuous film.

As shown in Fig. 9, J_{sc} of the NW array with the grating structure is smaller than that of the array with the flat layer. Larger portion of the grating surface is covered by the NWs as increasing the NW diameter. As a result, propagating SPP is seriously disturbed by the large sized NWs. As shown in Fig. 7, the grating-coupled SPP excitation occurs in the visible and NIR range, while varying the grating period from 600 to 1000 nm. At similar wavelength range, 400-nm-diameter NWs have several guided mode resonance and LSP-resonance peaks (Fig. 8). Thus, coupling among the photons related to the guided modes, LSPs, and SPPs will contribute to the optical characteristics of the large-diameter NW arrays.

VII. SUMMARY

We investigated influences of an Al back reflector on optical absorption and photocurrent of a vertical Si NW array solar cell. For a small-sized (diameter: 100 nm) and sparsely spaced (period: 800 nm) array, a flat Al underlayer beneath the Si NW array caused a LSP-induced peak in the NW absorption spectra. If the Al layer had a grating structure, grating-coupled SPPs and scattered light could affect the absorption spectra of the NWs. In planar solar cells, the role of the back reflector is limited to the increase of the optical path length in the absorber. In contrast, the back reflector can influence the optical characteristics of the NW devices, via

reflection of both light in NWs and light between NWs as well as plasmonic field confinement. According to the calculated optical absorption, the photocurrent of a 1-μm-thick, 400-nm-diameter, and 500-nm-period Si NW array with a 60-nm-thick flat Al back reflector can be 19.6 mA/cm^2, which is 45.2% larger than that of a 1-μm-thick planar Si device with a flat Al back reflector. These results provide a new perspective on short Si NW solar cells and other NW-based optoelectronic device applications.

ACKNOWLEDGMENTS

This work was supported by the Pioneer Research Center Program (2010-0002231) and the Quantum Metamaterials Research Center (2008-0061893) through the National Research Foundation of Korea Grant. This work was also supported by the New & Renewable Energy Technology Development Program of the Korea Institute of Energy Technology Evaluation and Planning (KETEP) Grant (20123010010160).

[1]K. Seo, M. Wober, P. Steinvurzel, E. Schonbrun, Y. Dan, T. Ellenbogen, and K. B. Crozier, Nano Lett. **11**, 1851 (2011).
[2]L. Cao, J. S. White, J.-S. Park, J. A. Schuller, B. M. Clemens, and M. L. Brongersma, Nature Mater. **8**, 643 (2009).
[3]C.-H. Cho, C. O. Aspetti, M. E. Turk, J. M. Kikkawa, S.-W. Nam, and R. Agarwal, Nature Mater. **10**, 669 (2011).
[4]X. Duan, Y. Huang, R. Agarwal, and C. M. Lieber, Nature **421**, 241 (2003).
[5]M. D. Kelzenberg, S. W. Boettcher, J. A. Petykiewicz, D. B. Turner-Evans, M. C. Putnam, E. L. Warren, J. M. Spurgeon, R. M. Briggs, N. S. Lewis, and H. A. Atwater, Nature Mater. **9**, 368 (2010).
[6]N. Huang, C. Lin, and M. L. Povinelli, J. Opt. **14**, 024004 (2012).
[7]H. Alaeian, A. C. Atre, and J. A. Dionne, J. Opt. **14**, 024006 (2012).
[8]A. Deinega and S. John, J. Appl. Phys. **112**, 074327 (2012).
[9]J. Li, H. Y. Yu, S. M. Wong, X. Li, G. Zhang, P. G.-Q. Lo, and D.-L. Kwong, Appl. Phys. Lett. **95**, 243113 (2009).
[10]C. Lin and M. L. Povinelli, Opt. Express **19**, A1148 (2011).
[11]Q. G. Du, C. H. Kam, H. V. Demir, H. Y. Yu, and X. W. Sun, Opt. Lett. **36**, 1884 (2011).
[12]B. C. P. Sturmberg, K. B. Dossou, L. C. Botten, A. A. Asatryan, C. G. Poulton, R. C. McPhedran, and C. M. de Sterke, Appl. Phys. Lett. **101**, 173902 (2012).
[13]B. C. P. Sturmberg, K. B. Dossou, L. C. Botten, A. A. Asatryan, C. G. Poulton, C. M. de Sterke, and R. C. McPhedranm, Opt. Express **19**, A1067 (2011).
[14]K.-T. Park, Z. Guo, H.-D. Um, J.-Y. Jung, J. M. Yang, S. K. Lim, Y. S. Kim, and J.-H. Lee, Opt. Express **19**, A41 (2011).
[15]E. Lee, Y. Kim, M. Gwon, D.-W. Kim, S.-H. Baek, and J. H. Kim, Sol. Energy Mater. Sol. Cells **103**, 93 (2012).
[16]K. Zhou, Z. Guo, X. Li, J.-Y. Jung, S.-W. Jee, K.-T. Park, H.-D. Um, N. Wang, and J.-H. Lee, Opt. Express **20**, A777 (2012).
[17]R. Ren, Y. Guo, and R. Zhu, Opt. Lett. **37**, 4245 (2012).
[18]J. K. Hyun and L. J. Lauhon, Nano Lett. **11**, 2731 (2011).
[19]S. Brittman, H. Gao, E. C. Garnett, and P. Yang, Nano Lett. **11**, 5189 (2011).
[20]P. Senanayake, C.-H. Hung, J. Shapiro, A. Scofield, A. Lin, B. S. Williams, and D. L. Huffaker, Opt. Express **20**, 25489 (2012).
[21]L.-W. Chou, N. Shin, S. V. Sivaram, and M. A. Filler, J. Am. Chem. Soc. **134**, 16155 (2012).
[22]J. P. Sundararajan, P. Bakharev, I. Niraula, B. A. F. Kengne, Q. MacPherson, M. Sargent, B. Hare, and D. N. McIlroy, Nano Lett. **12**, 5181 (2012).
[23]H. C. Jeon, C.-J. Heo, S. Y. Lee, and S.-M. Yang, Adv. Funct. Mater. **22**, 4268 (2012).
[24]J. Kim, E. Lee, M. Ju, H. Kim, J. Yi, S.-J. Moon, M. S. Hyun, and D.-W. Kim, Opt. Express **21**, A607 (2013).
[25]S. Mokkapati and K. R. Catchpole, J. Appl. Phys. **112**, 101101 (2012).
[26]S. A. Maier and H. A. Atwater, J. Appl. Phys. **98**, 011101 (2005).
[27]See http://www.lumerical.com/ for Lumerical Solutions, Inc.
[28]A. Taflove and S. C. Hagness, *Computational Electrodynamics: The Finite-Difference Time-Domain Method* (Artech House, Boston, 2005).
[29]I. Zorić, M. Zäch, B. Kasemo, and C. Langhammer, ACS Nano **5**, 2535 (2011).
[30]M. W. Knight, H. Sobhani, P. Nordlander, and N. J. Halas, Science **332**, 702 (2011).
[31]M. Gwon, E. Lee, D.-W. Kim, K.-J. Yee, M. J. Lee, and Y. S. Kim, Opt. Express **19**, 5895 (2011).